Structural Engineering and Mechanics, Vol. 24, No. 2 (2006) 227-245
DOI: http://dx.doi.org/10.12989/sem.2006.24.2.227

A compressible finite element model for hyperelastic members under different modes of deformation

M. C. Manna† and A. H. Sheikh‡

Department of Ocean Engineering and Naval Architecture, Indian Institute of Technology, Kharagpur – 721 302, India

R. Bhattacharyya‡†

Department of Mechanical Engineering, Indian Institute of Technology, Kharagpur – 721 302, India

(Received August 25, 2005, Accepted May 17, 2006)

Abstract. The performance of a three dimensional non-linear finite element model for hyperelastic material considering the effect of compressibility is studied by analyzing rubber blocks under different modes of deformation. It includes simple tension, pure shear, simple shear, pure bending and a mixed mode combining compression, shear and bending. The compressibility of the hyperelastic material is represented in the strain energy function. The nonlinear formulation is based on updated Lagrangian (UL) technique. The displacement model is implemented with a twenty node brick element having u, v and w as the degrees of freedom at each node. The results obtained by the present numerical model are compared with the analytical solutions available for the basic modes of deformation where the agreement between the results is found to be satisfactory. In this context some new results are generated for future references since the number of available results on the present problem is not sufficient enough.

Keywords: nonlinear finite element model; compressible strain energy function; hyperelastic material.

1. Introduction

The use of rubber as structural material is steadily gaining popularity due to some of its specific features. One of the significant advantages of the material is its ability to dissipate kinetic energy associated with impact, shock or any dynamic loading, which is much higher compared to other materials. The material has a large amount of deformability and it may be considered to be elastic in that range of deformation if Mullin's effect and permanent set are ignored. These unique features are exploited to solve many engineering problems in an elegant manner. The use of rubber as vibration isolators, shock absorbers, load bearing materials, sealant materials and filler between two railway lines are some of its important applications. The detailed applications are well documented in the text by Gent (2001).

† Mr., E-mail: mcm_naval@rediffmail.com
‡ Associate Professor, Corresponding author, E-mail: hamid@naval.iitkgp.ernet.in
‡† Professor, E-mail: rbmail@mech.iitkgp.ernet.in

On the other hand the rubber material is found to exhibit a near incompressible feature and this makes the prediction of stress and deformation quite difficult. Apart from that a good amount of complexity is involved in the solution of the problem due to severe nonlinearity induced by the extremely large deformations as mentioned above. Due to theses complexities, the analytical solution exists only for some elementary cases and its number is very few as expected. Therefore, a computer simulation is the only alternative for design optimization of a practical engineering component. In this context, the finite element method is most suitable since it is regarded as the most accurate, versatile and comprehensive numerical technique specifically in the field of computational solid mechanics.

It is to be noted that the truly incompressibility condition of rubber plays the most crucial role in finite element analysis when its bulk modulus becomes infinite and Poisson's ratio becomes 0.5. In some analytical solution the truly incompressibility condition is used to make the problem simple but it is not so in finite element analysis. In that situation, the complete state of stress can not be obtained from strain only since the hydrostatic pressure component can not produce any volumetric strain. Thus pressure is to be taken as a separate unknown along with the usual unknowns for the displacements and it leads to a mixed-field problem. Herrmann (1965) is one of the first investigators who identified the problem and proposed a formulation in terms of displacements and mean pressure. Apart from that a number of alternative attempts (Askes *et al*. 2004, Belytschko *et al.* 1994, Chen and Pan 1996, Chen *et al.* 2000, Kuhl *et al.* 2004, Liu *et al.* 1988, 1991, Masud and Xia 2005, Monaghan 1988, Nayroles *et al.* 1992, Sulsky *et al.* 1994, Zidi and Cheref 2002, Zienkiewicz 1977) have been made by different investigators to treat the incompressibility condition.

However, in reality, rubber is not completely incompressible (ν = 0.5), it is rather near incompressible i.e., a certain degree of compressibility exists though it is small. In this context, Obata (1974) has reported that the range of variation for the Poisson's ratio lies between from 0.49 to 0.4998 while Peng *et al.* (1994) has recommended a range of 0.498 to 0.4999. They have also mentioned that the Poisson's ratio of most of the industrial rubbers lies between 0.4985 and 0.4995. So the near incompressible feature ($\nu < 0.5$) helps us to use usual finite element model based on displacements since the critical condition at $\nu = 0.5$ is not reached. Thus someone can avoid the use of mixed-field formulation, which involves a number of difficulties as discussed by Gadala (1992). It is observed that the expanded global stiffness matrix does not become positive definite and it causes numerical difficulties especially in nonlinear analysis (Argyris *et al.* 1974). Again a mixed formulation does not work with any element and it requires different order of interpolation functions for the pressure and displacements, which involves computational difficulties (Argyris *et al.* 1974, Bathe 1982).

Thus, the obvious choice in this regard is the straightforward displacement finite element model but it should be mentioned that the model may suffer from numerical instability when the value of Poisson's ratio becomes very close to 0.5 (critical value) such as 0.499999. In such case the use of mixed-field formulation becomes essential and one of such studies is due to Sussman and Bathe (1987) where they took the value of Poisson's ratio up to 0.49999999. Anyway the displacement finite element model using the strain energy function of Peng and Chang (1997) proposed in the present study is found to work without any problem up to a value of $\nu = 0.4995$. Again it has been observed that the compressible finite element solution of Peng and Chang (1997) for $\nu = 0.499$ almost matches with the analytical solution for completely incompressible condition ($\nu = 0.5$). The above observations as well as the realistic range of values of Poisson's ratio have motivated the

authors to adopt the displacement finite element model. In the present study, the strain energy function of Peng and Chang (1997) is used since it gives a more realistic representation of near incompressible rubber elastic material and is well tested in single-field (displacement) finite element analysis.

The strain energy function as mentioned above is utilized to get the constitutive relation of rubber/ hyperelastic materials (Peng and Chang 1997). The state of strain is used to express the strain energy function, which is not dependent on the path of deformation. Again the state of strain is generally expressed with the three components of principal stretches (λ_1, λ_2 and λ_3) measured from a given configuration (Ogden 1972).

In the present study, the 3D brick element having twenty nodes is used to implement the proposed scheme consisting of geometric nonlinearity due to large deformation up to a considerable extent and constitutive equation based on strain energy function (Peng and Chang 1997) for rubbers/ elastomers. The updated Lagrangian (UL) technique based on Cauchy stress tensor and Almansi strain tensor is used for geometric nonlinearity. The formulation is purely displacement-based where each node contains three usual degrees of freedom *u*, *v* and *w*. The arc-length method (Crisfield 1981, de Souza Neto and Feng 1999) is used to solve the nonlinear problem utilizing the assembled incremental equilibrium equations appropriately. The stresses are computed at the Gauss points and extrapolated at the outer corner nodes according to Hinton and Campbell (1974) when it is required. The present numerical model is applied to solve problems of rubber blocks under simple tension, pure shear, simple shear, pure bending and a mixed mode combining compression, shear and bending. The results obtained are compared with the available analytical solutions for the basic modes of deformation. New results are also generated for future references since the number of available results on the present problem is very few.

2. Formulation

It has been mentioned that the present problem involves severe nonlinearity. In such case, the incremental solution scheme is most suitable where the entire loading path is divided into a number of steps. It gives different configurations/states such as ${}^0\Omega$, ${}^1\Omega$, ...${}^n\Omega$, ${}^{n+1}\Omega$, ..., where ${}^0\Omega$ is the initial state while ${}^n\Omega$ is any intermediate one. In this system, any displacement component u_i at two adjacent states may be expressed as

$$ {}^{n+1}u_i = {}^n u_i + u_i \qquad (i = 1, 2 \text{ and } 3) \tag{1} $$

where u_i is the increment of the displacement component ${}^n u_i$. In a similar manner the coordinates at any state may be obtained as

$$ {}^{n+1}x_i = {}^0 x_i + {}^{n+1}u_i \text{ or } {}^{n+1}x_i = {}^n x_i + u_i \tag{2} $$

Now the equilibrium equation of the body at any state may be obtained by utilizing the principle of virtual work. According to this principle, a compatible small virtual displacement is imposed on the body and the virtual work carried out by the internal forces/stresses is equated with that due to the external loads. Following the updated Lagrangian concept (Bathe 1982) the governing equation may be expressed as

$$\int \delta({}^{n+1}_{n}\varepsilon_{ij})\, {}^{n+1}_{n}\sigma_{ij}\, {}^{n}dV = {}^{n+1}P \tag{3}$$

where

$${}^{n+1}P = \int \delta({}^{n+1}u_k)\, {}^{n}\rho({}^{n+1}_{n}f_k)\, {}^{n}dV + \int \delta({}^{n+1}u_k)\, {}^{n+1}_{n}t_k\, {}^{n}dA \tag{4}$$

The different terms in the above Eqs. (3) and (4) are as follows:

$\delta({}^{n+1}_{n}\varepsilon_{ij})$ is the variation of Green-Lagrangian strain component ${}^{n+1}_{n}\varepsilon_{ij}$ at the $(n+1)$-th configuration, but measured in terms of the n-th configuration

${}^{n+1}_{n}\sigma_{ij}$ is the corresponding 2nd Piola Kirchhoff stress component

${}^{n}dV$ is the volume of an element at the n-th configuration

${}^{n}\rho$ is the density at the n-th configuration

${}^{n+1}_{n}f_k$ is the body force per unit mass at the $(n+1)$-th configuration, but measured in the n-th configuration

${}^{n+1}_{n}t_k$ is the surface force at the $(n+1)$-th configuration, but measured in the n-th configuration

${}^{n}dA$ is the surface area of an element at the n-th configuration

The above stress and strain components may be expressed with the help of an incremental decomposition as follows:

$${}^{n+1}_{n}\sigma_{ij} = {}^{n}_{n}\sigma_{ij} + \sigma_{ij} \tag{5}$$

$${}^{n+1}_{n}\varepsilon_{ij} = {}^{n}_{n}\varepsilon_{ij} + \varepsilon_{ij} \tag{6}$$

Since ${}^{n}_{n}\varepsilon_{ij} = 0$ in the above equation, it may be expressed by splitting the incremental part ε_{ij} into linear and nonlinear components as

$${}^{n+1}_{n}\varepsilon_{ij} = \varepsilon_{ij} = \varepsilon^{0}_{ij} + \varepsilon^{L}_{ij} \tag{7}$$

where

$$\varepsilon^{0}_{ij} = \frac{1}{2}\left(\frac{\partial u_i}{\partial({}^{n}x_j)} + \frac{\partial u_j}{\partial({}^{n}x_i)}\right), \quad \varepsilon^{L}_{ij} = \frac{1}{2}\left(\frac{\partial u_k}{\partial({}^{n}x_i)}\frac{\partial u_k}{\partial({}^{n}x_j)}\right) \tag{8}$$

Again ${}^{n}_{n}\sigma_{ij}$ is simply the Cauchy stress ${}^{n}\tau_{ij}$ and with this, Eq. (5) becomes

$${}^{n+1}_{n}\sigma_{ij} = {}^{n}\tau_{ij} + \sigma_{ij} \tag{9}$$

The Cauchy stress and the incremental stress in the above equation may be obtained as:

$${}^{n}\tau_{ij} = {}_{n}C_{ijkl}\, {}^{n}e_{kl} \tag{10}$$

$$\sigma_{ij} = {}_{n}C_{ijkl}\varepsilon_{kl} \tag{11}$$

In the above equation ${}_{n}C_{ijkl}$ is the component of the constitutive tensor and ${}^{n}e_{kl}$ is that of Almansi strain tensor at the n-th configuration. For rubber material ${}_{n}C_{ijkl}$ is obtained from its strain energy

density function to be presented later. The component of Almansi strain tensor may be defined as

$$ {}^{n}e_{kl} = \frac{1}{2}\left(\frac{\partial({}^{n}u_k)}{\partial({}^{n}x_l)} + \frac{\partial({}^{n}u_l)}{\partial({}^{n}x_k)} - \frac{\partial({}^{n}u_r)}{\partial({}^{n}x_k)}\frac{\partial({}^{n}u_r)}{\partial({}^{n}x_l)} \right) \tag{12} $$

After substitution of Eqs. (7), (9) and (11) in Eq. (3) it becomes

$$ \int \delta(\varepsilon_{ij})_n C_{ijkl} \varepsilon_{kl}^{\,n} dV + \int \delta(\varepsilon_{ij}^{L})^n \tau_{ij}^{\,n} dV = {}^{n+1}P - \int \delta(\varepsilon_{ij}^{0})^n \tau_{ij}^{\,n} dV \tag{13} $$

As the above equation can not be solved due to the presence of nonlinear incremental strains, it is linearized by taking $\delta(\varepsilon_{ij}) = \delta(\varepsilon_{ij}^{0})$ and $\varepsilon_{kl} = \varepsilon_{kl}^{0}$ to get an approximate solution. With these the above equation becomes

$$ \int \delta(\varepsilon_{ij}^{0})_n C_{ijkl} \varepsilon_{kl}^{0\,n} dV + \int \delta(\varepsilon_{ij}^{L})^n \tau_{ij}^{\,n} dV = {}^{n+1}P - \int \delta(\varepsilon_{ij}^{0})^n \tau_{ij}^{\,n} dV \tag{14} $$

Since $\delta({}^{n+1}u_k) = \delta(u_k)$, the virtual work due to external loads ${}^{n+1}P$ as presented in (4) may be rewritten as

$$ {}^{n+1}P = \int \delta(u_k)^n \rho({}^{n+1}_{n}f_k)^n dV + \int \delta(u_k)^{n+1}_{n}t_k^{\,n} dA \tag{15} $$

The above Eqs. (14) and (15) may be presented in matrix form with the help of Eq. (8) as

$$ \int \delta\{\hat{\varepsilon}^0\}^T [{}_n\tilde{C}] \{\hat{\varepsilon}^0\}^n dV + \int \delta\{\hat{\theta}\}^T [{}^n\tilde{\tau}_{ij}] \{\hat{\theta}\}^n dV = {}^{n+1}P - \int \delta\{\hat{\varepsilon}^0\}^T \{{}^n\hat{\tau}_{ij}\}^n dV \tag{16} $$

$$ {}^{n+1}P = \int \delta\{\hat{u}\}^T {}^n\rho\{{}^{n+1}_{n}\hat{f}\}^n dV + \int \delta\{\hat{u}\}^T \{{}^{n+1}_{n}\hat{t}\}^n dA \tag{17} $$

where the different matrices in the above Eqs. (16) and (17) are:

$$ \{\hat{u}\} = \{u_1 \;\; u_2 \;\; u_3\}^T $$

$$ \{{}^{n+1}_{n}\hat{f}\} = \{{}^{n+1}_{n}f_1 \;\; {}^{n+1}_{n}f_2 \;\; {}^{n+1}_{n}f_3\}^T $$

$$ \{{}^{n+1}_{n}\hat{t}\} = \{{}^{n+1}_{n}t_1 \;\; {}^{n+1}_{n}t_2 \;\; {}^{n+1}_{n}t_3\}^T $$

$$ \{\hat{\varepsilon}^0\} = \{\varepsilon_{11}^0 \;\; \varepsilon_{22}^0 \;\; \varepsilon_{33}^0 \;\; 2\varepsilon_{12}^0 \;\; 2\varepsilon_{23}^0 \;\; 2\varepsilon_{31}^0\}^T $$

$$ [{}_n\tilde{C}] = \begin{bmatrix} {}_nC_{1111} & {}_nC_{1122} & {}_nC_{1133} & {}_nC_{1112} & {}_nC_{1123} & {}_nC_{1131} \\ {}_nC_{2211} & {}_nC_{2222} & {}_nC_{2233} & {}_nC_{2212} & {}_nC_{2223} & {}_nC_{2231} \\ {}_nC_{3311} & {}_nC_{3322} & {}_nC_{3333} & {}_nC_{3312} & {}_nC_{3323} & {}_nC_{3331} \\ {}_nC_{1211} & {}_nC_{1222} & {}_nC_{1233} & {}_nC_{1212} & {}_nC_{1223} & {}_nC_{1231} \\ {}_nC_{2311} & {}_nC_{2322} & {}_nC_{2333} & {}_nC_{2312} & {}_nC_{2323} & {}_nC_{2331} \\ {}_nC_{3111} & {}_nC_{3122} & {}_nC_{3133} & {}_nC_{3112} & {}_nC_{3123} & {}_nC_{3131} \end{bmatrix} $$

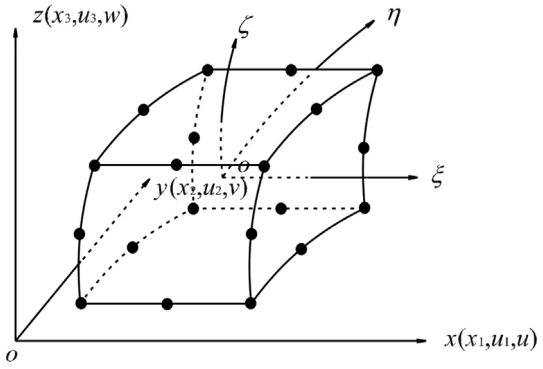

Fig. 1 A twenty noded 3D brick element

$$\{\hat{\theta}\} = \left\{ \frac{\partial u_1}{\partial({}^n x_1)} \quad \frac{\partial u_1}{\partial({}^n x_2)} \quad \frac{\partial u_1}{\partial({}^n x_3)} \quad \frac{\partial u_2}{\partial({}^n x_1)} \quad \frac{\partial u_2}{\partial({}^n x_2)} \quad \frac{\partial u_2}{\partial({}^n x_3)} \quad \frac{\partial u_3}{\partial({}^n x_1)} \quad \frac{\partial u_3}{\partial({}^n x_2)} \quad \frac{\partial u_3}{\partial({}^n x_3)} \right\}^T$$

$$[{}^n\tilde{\tau}] = \begin{bmatrix} [{}^n\tau] & 0 & 0 \\ 0 & [{}^n\tau] & 0 \\ 0 & 0 & [{}^n\tau] \end{bmatrix}, \quad [{}^n\tau] = \begin{bmatrix} {}^n\tau_{11} & {}^n\tau_{12} & {}^n\tau_{13} \\ {}^n\tau_{21} & {}^n\tau_{22} & {}^n\tau_{23} \\ {}^n\tau_{31} & {}^n\tau_{32} & {}^n\tau_{33} \end{bmatrix}$$

$$[{}^n\hat{\tau}] = \{ {}^n\tau_{11} \quad {}^n\tau_{22} \quad {}^n\tau_{33} \quad {}^n\tau_{12} \quad {}^n\tau_{23} \quad {}^n\tau_{31} \}^T$$

Eqs. (16) and (17) are in convenient form for the finite element implementation, where the twenty noded 3D brick element (Fig. 1) based on isoparametric formulation is used. According to isoparametric formulation the displacements and geometry at n-th configuration can be represented with same interpolation functions (Bathe 1982, Cook *et al.* 2001) as

$${}^n x_i = \sum_{k=1}^{20} N^k(\xi, \eta, \zeta) {}^n x_i^k, \quad {}^n u_i = \sum_{k=1}^{20} N^k(\xi, \eta, \zeta) {}^n u_i^k \tag{18}$$

where $N^k(\xi, \eta, \zeta)$ or simply N^k is the interpolation function corresponding to k-th node, while ${}^n x_i^k$ and ${}^n u_i^k$ are the coordinate and displacement at the corresponding node. In a similar manner the incremental displacements can be expressed as

$$u_i = \sum_{k=1}^{20} N^k u_k^i \tag{19}$$

With these Eqs. (18) and (19) along with (8), the incremental strain vectors $\{\hat{\varepsilon}^0\}$ and $\{\hat{\theta}\}$ in (16) and the incremental displacement vector $\{\hat{u}\}$ in (17) may be expressed in terms of incremental nodal displacement vector $\{U\}$ as

$$\{\hat{\varepsilon}^0\} = [[B_0^1] \; [B_0^2] \; [B_0^3] \; \dots \; [B_0^k] \; \dots \; [B_0^{20}]]\{U\} = [B_0]\{U\} \tag{20}$$

$$\{\hat{\theta}\} = [[B_G^1] \; [B_G^2] \; [B_G^3] \; \dots \; [B_G^k] \; \dots \; [B_G^{20}]]\{U\} = [B_G]\{U\} \tag{21}$$

$$\{\hat{u}\} = [[\bar{N}^1]\ [\bar{N}^2]\ [\bar{N}^3]\ \ldots\ [\bar{N}^k]\ \ldots\ [\bar{N}^{20}]]\{U\} = [\bar{N}]\{U\} \tag{22}$$

where

$$\{U\} = \{u_1^1\ u_2^1\ u_3^1\ u_1^2\ u_2^2\ u_3^2\ \ldots\ u_1^{20}\ u_2^{20}\ u_3^{20}\}^T$$

$$[B_0^k] = \begin{bmatrix} \dfrac{\partial N^k}{\partial^n x_1} & 0 & 0 & \dfrac{\partial N^k}{\partial^n x_2} & 0 & \dfrac{\partial N^k}{\partial^n x_3} \\ 0 & \dfrac{\partial N^k}{\partial^n x_2} & 0 & \dfrac{\partial N^k}{\partial^n x_1} & \dfrac{\partial N^k}{\partial^n x_3} & 0 \\ 0 & 0 & \dfrac{\partial N^k}{\partial^n x_3} & 0 & \dfrac{\partial N^k}{\partial^n x_2} & \dfrac{\partial N^k}{\partial^n x_1} \end{bmatrix}^T$$

$$[B_G^k] = \begin{bmatrix} \dfrac{\partial N^k}{\partial^n x_1} & \dfrac{\partial N^k}{\partial^n x_2} & \dfrac{\partial N^k}{\partial^n x_3} & 0 & 0 & 0 & 0 & 0 & 0 \\ 0 & 0 & 0 & \dfrac{\partial N^k}{\partial^n x_1} & \dfrac{\partial N^k}{\partial^n x_2} & \dfrac{\partial N^k}{\partial^n x_3} & 0 & 0 & 0 \\ 0 & 0 & 0 & 0 & 0 & 0 & \dfrac{\partial N^k}{\partial^n x_1} & \dfrac{\partial N^k}{\partial^n x_2} & \dfrac{\partial N^k}{\partial^n x_3} \end{bmatrix}^T$$

$$[\bar{N}^k] = \begin{bmatrix} N^k & 0 & 0 \\ 0 & N^k & 0 \\ 0 & 0 & N^k \end{bmatrix}$$

After substitution of Eqs. (20), (21) and (22) in (16) and (17) and subsequent necessary rearrangement the incremental equilibrium equation may be obtained in its final form as

$$[K_T]\{U\} = \{^{n+1}R\} - \{^{n+1}F\} \tag{23}$$

where

$$[K_T] = \int([B_0]^T[{}_n\tilde{C}][B_0] + [B_G]^T[{}^n\tilde{\tau}][B_G])^n dV$$

$$\{^{n+1}R\} = \int[\bar{N}]^T {}^n\rho\{{}^{n+1}_n\hat{f}\}^n dV + \int[\bar{N}]^T\{{}^{n+1}_n\hat{\tau}\}^n dA$$

$$\{^{n+1}F\} = \int[B_0]^T\{{}^n\hat{\tau}\}^n dV$$

Following the usual technique, integration of these quantities is carried out numerically according to Gauss quadrature integration rule where the number of Gauss points taken in all the three directions is 3.

The technique to evaluate the components of the constitutive tensor ${}_nC_{ijkl}$ of the rubber material will now be presented. In the present study the material models used are: Neo-Hookean, Mooney-

Rivlin and Ogden-Tschoegl. In this context, the strain energy density function W of Peng and Chang (1997), which is expressed in terms of principal stretches (λ_1, λ_2, λ_3) as

$$W = \sum_{k=1}^{m} \mu_k \left(\frac{\lambda_1^{\alpha_k} + \lambda_2^{\alpha_k} + \lambda_3^{\alpha_k} - 3}{\alpha_k} - \ln J \right) + \frac{\lambda}{81}(9 \ln J + J^{-9} - 1) \tag{24}$$

where μ_k and α_k are material constants, $J = \lambda_1 \lambda_2 \lambda_3$, $m = 1$, 2 or 3 depending on the material model (Ogden 1972, 1984) and the Lame's constant $\lambda = 2G\nu/(1 - 2\nu)$ where $G = \mu_k \alpha_k$. The values of the principal stretches λ_i and their directions v_{ij} are obtained from the left Cauchy-Green deformation tensor $[B]$ defined in terms of the deformation gradient $[{}_0^nX]$ as,

$$[B] = [{}_0^nX][{}_0^nX]^T \tag{25}$$

where $[{}_0^nX] = \begin{bmatrix} \frac{\partial^n x_1}{\partial^0 x_1} & \frac{\partial^n x_1}{\partial^0 x_2} & \frac{\partial^n x_1}{\partial^0 x_3} \\ \frac{\partial^n x_2}{\partial^0 x_1} & \frac{\partial^n x_2}{\partial^0 x_2} & \frac{\partial^n x_2}{\partial^0 x_3} \\ \frac{\partial^n x_3}{\partial^0 x_1} & \frac{\partial^n x_3}{\partial^0 x_2} & \frac{\partial^n x_3}{\partial^0 x_3} \end{bmatrix}$

The matrix $[B]$ may be expressed in terms of the principal stretches λ_i and their directions v_{ij} as

$$[B] = \begin{bmatrix} v_{11} & v_{21} & v_{31} \\ v_{12} & v_{22} & v_{32} \\ v_{13} & v_{23} & v_{33} \end{bmatrix} \begin{bmatrix} \lambda_1^2 & 0 & 0 \\ 0 & \lambda_2^2 & 0 \\ 0 & 0 & \lambda_3^2 \end{bmatrix} \begin{bmatrix} v_{11} & v_{12} & v_{13} \\ v_{21} & v_{22} & v_{23} \\ v_{31} & v_{32} & v_{33} \end{bmatrix} = [v][L][v]^T \tag{26}$$

where $[v]$ and $[L]$ are the eigenvector and eigenvalue matrices of $[B]$ respectively.

From the strain energy density function W in (24), the principal values of the Cauchy stress can be obtained (Ogden 1984) as

$${}^n t_i = \frac{\lambda_i}{J}\frac{\partial W}{\partial \lambda_i} = \frac{1}{J}\sum_{k=1}^{m} \mu_k (\lambda_i^{\alpha_k} - 1) + \frac{\lambda}{9}\left(\frac{1}{J} - \frac{1}{J^{10}}\right) \tag{27}$$

Using the above Eqs. (24) to (27), the components of constitutive tensor ${}_nC_{ijkl}$ may be obtained (Ogden 1984) as

$${}_nC_{ijkl} = \sum_{p=1}^{3}\sum_{q=1}^{3}\sum_{r=1}^{3}\sum_{s=1}^{3} v_{ip} v_{jq} L_{pqrs} v_{kr} v_{ls} \tag{28}$$

where, ${}_nL_{kkkk} = \lambda_k \frac{\partial^n t_k}{\partial \lambda_k} - {}^n t_k$, ${}_nL_{kkjj} = \lambda_j \frac{\partial^n t_k}{\partial \lambda_j} + {}^n t_k$, ${}_nL_{klkl} = \frac{{}^n t_k \lambda_l^2 - {}^n t_k \lambda_k^2}{\lambda_k^2 - \lambda_l^2}$, for $\lambda_k^2 \neq \lambda_l^2$ and ${}_nL_{klkl} = \frac{1}{2J}\sum_{i=1}^{m} \mu_i \alpha_i \lambda_k^{\alpha_i} - {}^n t_k$ for $\lambda_k^2 = \lambda_l^2$.

Table 1 Material constants of different material models

Material model	m	μ_1 (MPa)	μ_2 (MPa)	μ_3 (MPa)	α_1	α_2	α_3	ν
Neo-Hookean	1	0.618			2.0			0.49932
Mooney-Rivlin	2	0.367	–0.0292		2.0	–2.0		0.49932
Ogden-Tschoegl	3	0.618	0.001245	–0.00982	1.3	5.0	–2.0	0.49932

3. Results and discussions

In this section, numerical examples of rubber blocks are solved by the proposed finite element model to check its accuracy and range of applicability. For the purpose of validation, the analysis is first carried out for the basic modes of deformation, which includes simple tension, pure shear, simple shear and pure bending. The results obtained in all these cases are compared with the analytical solution. Finally an example having mixed mode deformation combining compression, shear and bending is analyzed and the results obtained are reported. In most of the cases, the material models of Ogden-Tschoegl, Mooney-Rivlin and neo-Hookean are used. The material constants of these models as shown in Table 1 are used in the present analysis unless specified otherwise.

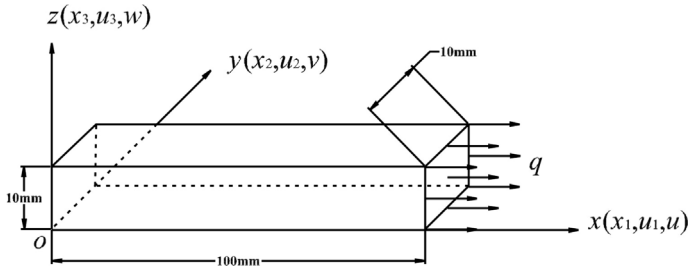

Fig. 2 A bar under simple tension

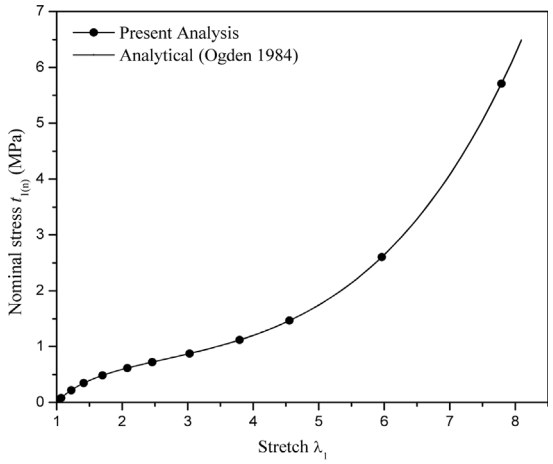

Fig. 3 Variation of nominal stress $t_{1(n)}$ with respect to stretch λ_1 of a bar under simple tension (Ogden-Tschoegl material)

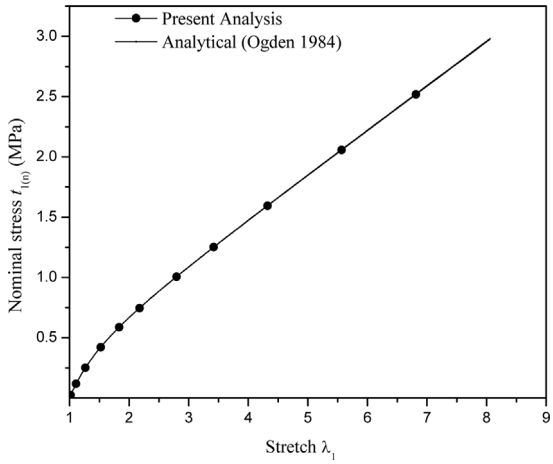

Fig. 4 Variation of nominal stress $t_{1(n)}$ with respect to stretch λ_1 of a bar under simple tension (Mooney-Rivlin material)

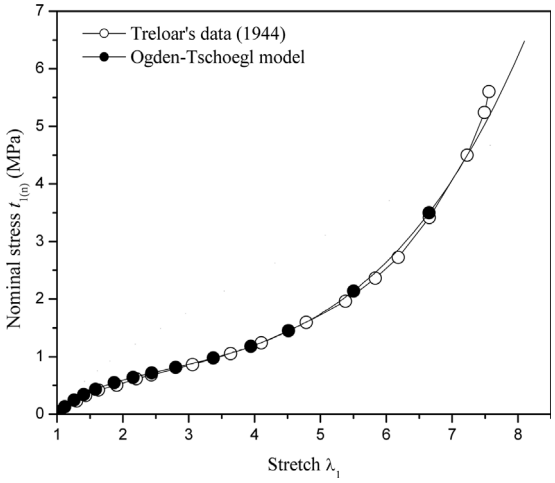

Fig. 5 Variation of nominal stress $t_{1(n)}$ with respect to stretch λ_1 of a bar under simple tension

3.1 Simple tension of a rectangular prismatic bar

A hyperelastic bar (Fig. 2) under axial tension is analyzed by the proposed finite element model using a mesh size of 10 × 1 × 1 (number of divisions along x, y and z are 10, 1 and 1 respectively) i.e., 10 elements. For the axial tension a uniformly distributed load is applied on the face at x = 100 mm where the load is consistently distributed at all the nodes on that face. On the opposite face (x = 0) the displacement components u (u_1) of all the nodes are restrained. Apart from that, the displacement components v (u_2) and w (u_3) at the faces y = 0 and z = 0, respectively, are restrained. The results obtained in the present analysis are plotted in Figs. 3 and 4 where the variation of the nominal (engineering) stress ($t_{1(n)} = {}^{n}\tau_{11}/\lambda_1$) is shown with respect to the major principal stretch. It is found that the value of $t_{1(n)}$ as well as λ_1 does not vary from point to point at any configuration/ load level as expected. The results are compared with the analytical solution based on original strain energy function (Ogden 1984) in these figures, which show an excellent agreement between them. For this mode of deformation, the analytical solution (Ogden 1984) used is given as $t_{1(n)} = {}^{n}\tau_{11}/\lambda_1 = \sum_{k=1}^{m} \mu_k(\lambda_1^{\alpha_k - 1} - \lambda_1^{-0.5\alpha_k - 1})$. The present results obtained for the Ogden-Tschoegl model are also plotted in Fig. 5 along with the experimental results of Treloar (1974) and it is observed that a good agreement exists between the two up to a stretch of 7.5.

3.2 Pure shear - a thin long plate under lateral tension

The problem of a thin infinitely long plate subjected to uniform lateral tension along the width is considered in this example. As it may be treated as plane strain problem, the analysis of a strip is sufficient to get the solution. For this purpose the same bar taken in the previous example (Fig. 2) is used as the required strip in the present case. Similar to the previous case, the analysis is carried out with an identical mesh size, loading and boundary conditions where one additional condition is imposed by restraining v (u_2) on the face at y = 10 mm. It should be noted that the present problem

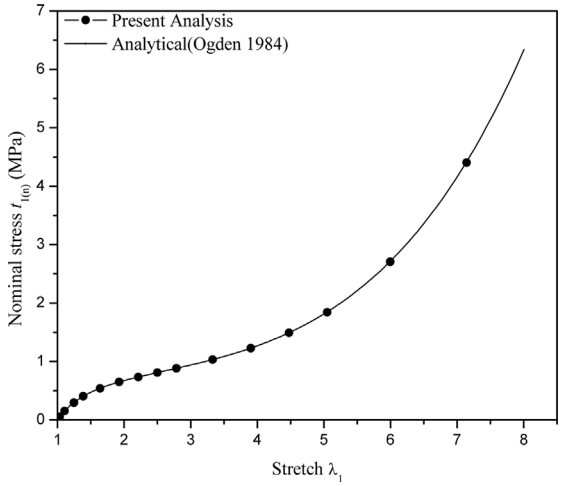

Fig. 6 Variation of nominal stress $t_{1(n)}$ with respect to stretch λ_1 of a thin long plate under lateral tension – pure shear (Ogden-Tschoegl material)

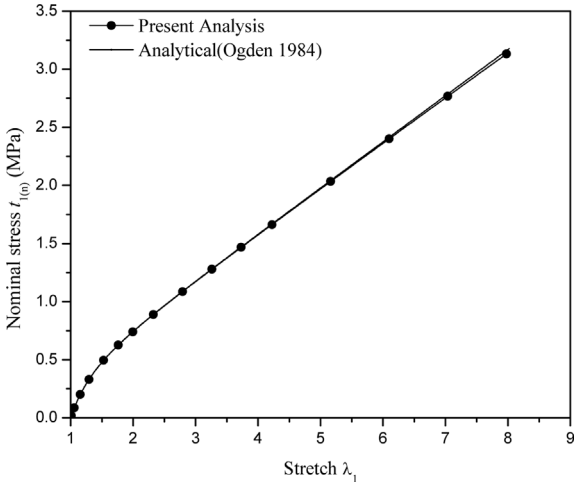

Fig. 7 Variation of nominal stress $t_{1(n)}$ with respect to stretch λ_1 of a thin long plate under lateral tension – pure shear (Mooney-Rivlin material)

can also be defined as a pure shear problem since the principal stretch along y direction is unity and stress along z direction is zero. In Figs. 6 and 7, the results are plotted in similar manner and compared with the analytical solution where the results are found to be exactly matching. For the case of pure shear, the analytical solution used (Ogden 1984) is $t_{1(n)} = \sum_{k=1}^{3} \mu_k (\lambda_1^{\alpha_k - 1} - \lambda_1^{-\alpha_k - 1})$.

3.3 Simple shear of a square plate

The simple shear of a square plate, as shown in Fig. 8, is studied in this example. The uniform shear load is applied on the face at x = 100 mm towards z direction where the load is as usual

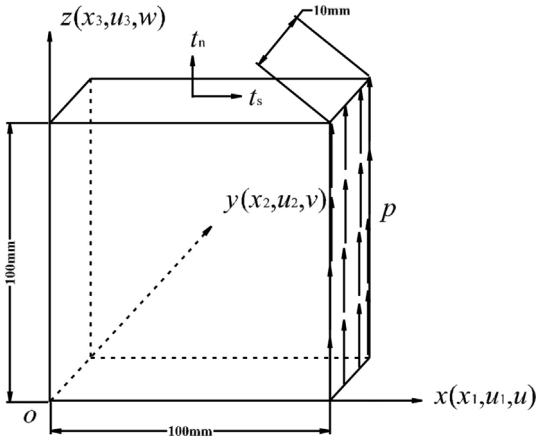

Fig. 8 A square plate under simple shear

Table 2 Different stress components in the square plate under simple shear

Shear strain γ	Sources	τ_{xx} (N/m^2)	τ_{yy} (N/m^2)	τ_{zz} (N/m^2)	τ_{xz} (N/m^2)	t_s (N/m^2)	t_n (N/m^2)
10^0	Analytical*	0.0000	0.0000	19214.4	108970	105684	–18635.0
	Present	0.0000	0.0000	19214.4	108970	105684	–18635.0
20^0	Analytical	0.0000	0.0000	81869.1	224934	198621	–72292.3
	Present	0.0000	0.0000	81869.1	224934	198621	–72292.3
30^0	Analytical	0.0000	0.0000	206000	356802	267602	–154500
	Present	0.0000	0.0000	206000	356802	267602	–154500
40^0	Analytical	0.0000	0.0000	435127	518564	304306	–255343
	Present	0.0000	0.0000	435127	518564	304306	–255343
50^0	Analytical	0.0000	0.0000	877731	736504	304306	–362657
	Present	0.0000	0.0000	877731	736504	304306	–362657
60^0	Analytical	0.0000	0.0000	0.185400E+07	0.107041E+07	267602	–463500
	Present	0.0000	0.0000	0.185400E+07	0.107041E+07	267602	–463500

*Beatty (1987)

distributed consistently at all the nodes on that face. For the imposition of the boundary conditions, the different displacement components restrained are: $u = 0$ at $x = 0$ mm, $x = 100$ mm, $z = 0$ mm and $z = 100$ mm; $v = 0$ at all the nodes; $w = 0$ at $x = 0$ mm. Taking the neo-Hookean material model, the analysis is carried out with 100 elements (mesh size: $10 \times 1 \times 10$). The results obtained in the form of stress components ($\tau_{xx} = {}^n\tau_{11}$, $\tau_{yy} = {}^n\tau_{22}$, $\tau_{zz} = {}^n\tau_{33}$ and $\tau_{xz} = {}^n\tau_{13}$) as well as normal and shear stresses (t_s and t_n) at the inclined edge ($z = 0$ or $z = 100$ mm) evaluated from these stresses are presented with those obtained from the analytical solution (Beatty 1987) for different values of shear strain ($\gamma = 2{}^n_0\varepsilon_{13}$) in Table 2. It clearly shows that the results obtained from both the sources are exactly matching.

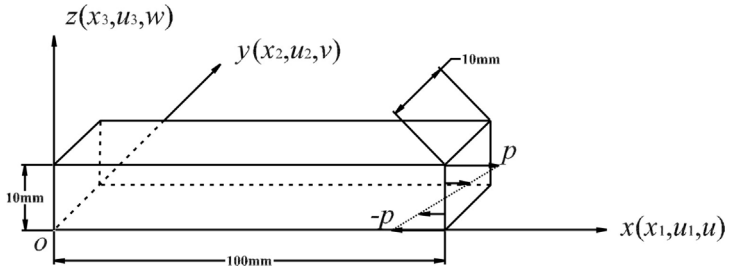

Fig. 9 A cantilever beam under pure bending

Table 3 Tip deflection of the cantilever beam under pure bending (neo-Hookean material)

End moment	Analytical (Ogden 1984)	Present
15 N-m	1.216 m	1.218 m
30 N-m	1.349 m	1.363 m

Table 4 Tip deflection of the cantilever beam under pure bending (Mooney-Rivlin material)

End moment	Analytical (Ogden 1984)	FEM-I[a] (Chen and Wu 1996)	FEM-II[b] (Chen and Wu 1996)	Present
12.5 N-m	1.392 m	1.320 m	1.226 m	1.395 m
25.0 N-m	0.950 m	-	-	0.959 m

[a]Finite Element Method (Regular mesh)
[b]Finite Element Method (Irregular mesh)

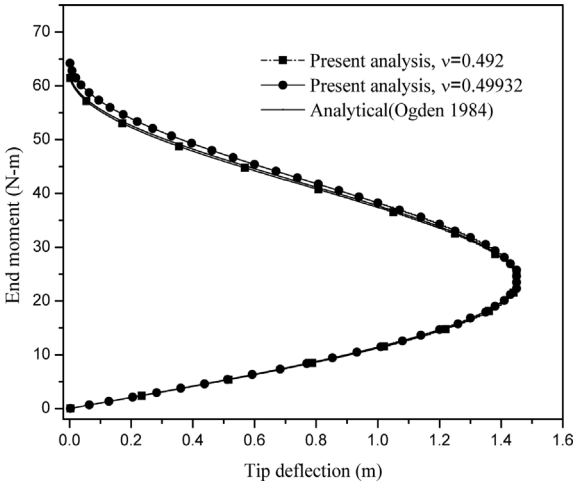

Fig. 10 Variation of end moment with respect to tip deflection of the cantilever beam under pure bending (neo-Hookean material)

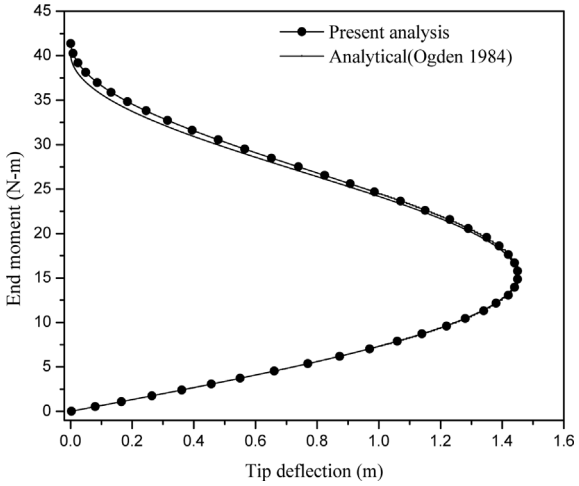

Fig. 11 Variation of end moment with respect to tip deflection of the cantilever beam under pure bending (Mooney-Rivlin material)

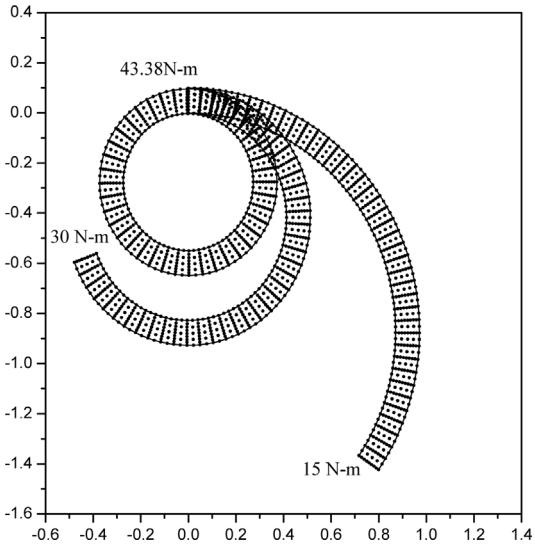

Fig. 12 Deformed configurations of the cantilever beam under pure bending due to different end moments (Ogden-Tschoegl material)

3.4 Pure bending of a cantilever beam

The case of pure bending is studied by taking a 2000 mm long elastomer cantilever beam having a square cross-section of 100 mm sides (Fig. 9) under the action of a moment at the free end. As 3D finite element is used in the present analysis, the moment is replaced by an equivalent normal load having linear variation across the depth. The boundary conditions imposed are: $u = 0$ at $x = 0$ mm, $v = 0$ at all the nodes and $w = 0$ at $x = 0$ mm and $z = 0$ mm. The analysis is carried out with 160 elements (mesh size: $40 \times 1 \times 4$) and the results obtained are presented in different forms. For neo-Hookean material, the tip deflection due to end moment of 15N-m and 30N-m evaluated in the present analysis are presented with those obtained from analytical solution (Ogden 1984) in Table 3. In a similar manner, the results are given for end moment of 12.5N-m and 25N-m in Table 4 for the Mooney-Rivlin material where the finite element results of Chen *et al.* (1996) for end moment of 12.5N-m are also included. The tables show that the present results are reasonably close to the analytical solution. Again, the variation of an end moment with respect to the tip deflection is plotted in Fig. 10 and Fig. 11 for these two materials where a close agreement between the results is similarly found. For the neo-Hookean material, the analysis is also carried out with a Poison's ratio of 0.492 and the results obtained are included in Fig. 11. Interestingly, it is found to be more close to the analytical solution than that obtained with 0.49932 as the value of Poison's ratio usually taken. Finally the deformed shapes of the beam for the Ogden-Tschoegl material are presented in Fig. 12 corresponding to different end moments.

3.5 A cantilever beam under inclined tip load

As the number of available results on deformation of rubber member is very few, a new problem is fabricated in this example. It is a cantilever beam subjected to an inclined tip load distributed uniformly at the free end (Fig. 13), which induces a combined mode of deformation that consists of compression, bending about y axis and shear in x-z plane. The analysis is carried out with 100 elements (mesh size: $5 \times 1 \times 20$) taking the neo-Hookean material. The boundary conditions taken

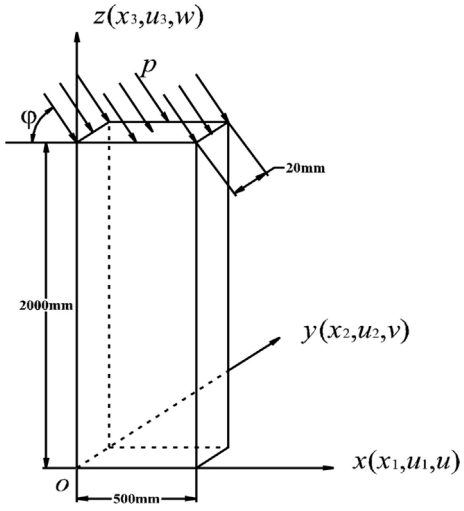

Fig. 13 A cantilever beam subjected to uniformly distributed inclined tip load

Table 5 Horizontal tip deflections (m) of the cantilever beam subjected to an inclined tip load (p = 25 kN/sq·m)

$\phi = 0^0$	$\phi = 15^0$	$\phi = 30^0$	$\phi = 45^0$	$\phi = 60^0$	$\phi = 75^0$
1.1461	1.0650	0.9317	0.7503	0.5278	0.2726

Table 6 Stress components (MPa) at the extreme fibers of the supported end of the cantilever beam subjected to an inclined tip load (p = 25 kN/sq·m)

ϕ	x = 0 mm, z = 0 mm				x = 500 mm, z = 0 mm			
	τ_{xx}	τ_{yy}	τ_{zz}	τ_{xy}	τ_{xx}	τ_{yy}	τ_{zz}	τ_{xy}
0°	0.7199	0.7322	0.7608	–0.1929	–0.9987	–0.9761	–0.9734	–0.1292
15°	0.6330	0.6424	0.6617	–0.1658	–0.8800	–0.8605	–0.8572	–0.1209
30°	0.5200	0.5260	0.5365	–0.1319	–0.7245	–0.7094	–0.7052	–0.1089
45°	0.3903	0.3933	0.3973	–0.0946	–0.5540	–0.5435	–0.5391	–0.0924
60°	0.2504	0.2511	0.2516	–0.0563	–0.3821	–0.3759	–0.3722	–0.0722
75°	0.1022	0.1020	0.1015	–0.0189	–0.2139	–0.2113	–0.2091	–0.0464

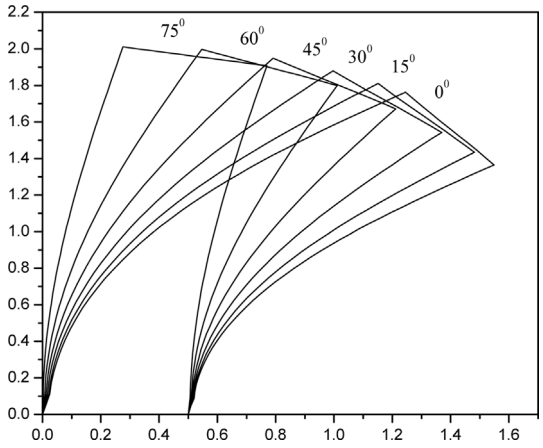

Fig. 14 Deformed configurations of the cantilever beam due an inclined load (25 kN/sq·m)

are: u = 0 at z = 0 mm, v = 0 at all the nodes and w = 0 at z = 0 mm. For the inclined load having an intensity of 25 kN/sq·m, the horizontal tip deflections obtained for different inclination ϕ of the load (Fig. 13) ranging from 0^0 to 75^0 are presented in Table 5. In a similar manner the stress components obtained at the extreme fibers of the supported end are presented in Table 6. Finally its deformed shape due to a 25 kN/sq·m inclined load with different values of ϕ is shown in Fig. 14.

3.6 A hollow cylinder subjected to an internal pressure, internal tangential distributed load and end surface distributed load

For same reason as mentioned in the previous example, another new problem is fabricated in this example. This is a circular rubber cylinder (Fig. 15) of an inner radius 0.1 m, an outer radius 0.25 m and a length 0.3 m which is subjected to an internal pressure (p_i), a distributed tangential load (p_t) at the inner cylindrical surface and a distributed linearly varying load (as shown in Fig. 15) at the end

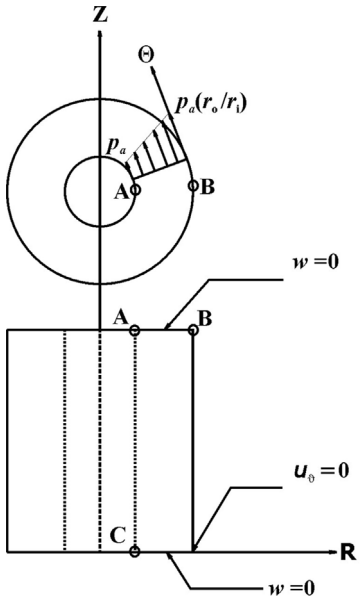

Fig. 15 A hollow cylinder

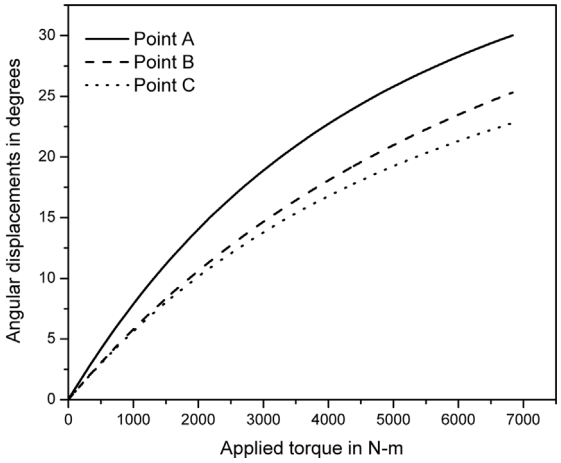

Fig. 16 Angular displacements versus total applied torque

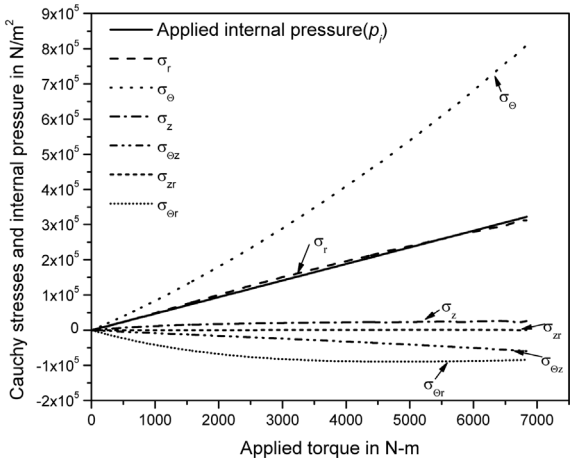

Fig. 17 Cauchy stresses at inner surface at $z = 0.15$ m and internal pressure vs. applied torque

surface at $Z = 0.3$ m where $p_a = \frac{1}{10} p_t$. The last two distributed loads result in a torque. The analysis is performed with 288 elements (mesh size: $6 \times 12 \times 4$) with 6 divisions along the R-direction, 12 divisions along the θ-direction and 4 divisions along the Z-direction. The boundary conditions imposed are: $w = 0.0$ at $Z = 0$ and $Z = 0.3$ m, $u_\theta = 0$ at $R = 0.25$ m and $Z = 0.0$. The angular displacements of point A, B and C about the z-axis are presented in Fig. 16. The rubber material is the Mooney-Rivlin type as mentioned in Table 1. The Cauchy stresses at inner cylindrical surface at $Z = 0.15$ m and the internal pressure variations are depicted in Fig. 17. From the graph it is seen that the internal pressure is in good agreement with the radial stress (σ_r) as expected.

3.7 A hollow cylinder under combined torsion and telescopic shearing

The hollow cylinder as taken in the previous example (Fig. 15) is considered for the problem of combined torsion and telescopic shearing. Uniformly distributed tangential and axial forces are applied on the inner cylindrical surface to simulate a torque and an axial load on the cylinder. The outer cylindrical surface is fixed and the inner cylindrical surface is restrained from radial displacement (u_θ). The cylinder is divided into 288 elements with 6 divisions along the R-direction, 12 divisions along the θ-direction and 4 divisions along the Z-direction. Radial stress (σ_{rr}), circumferential stress ($\sigma_{\theta\theta}$) and axial stress (σ_{zz}) vs. radius for different angles of twist (φ) and axial displacements (w) are shown in Figs. 18, 19 and 20 respectively.

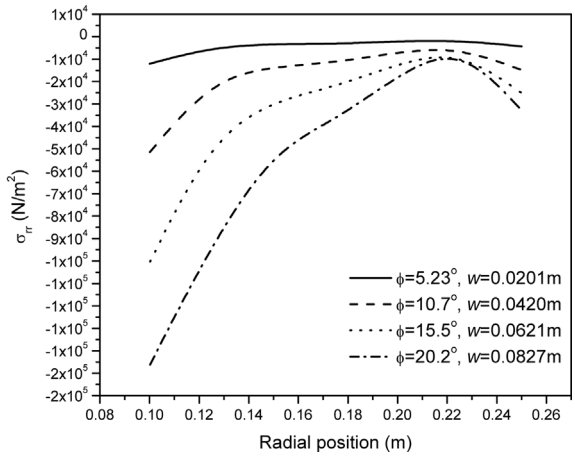

Fig. 18 Radial stress versus radius for different angles of twist and axial displacements

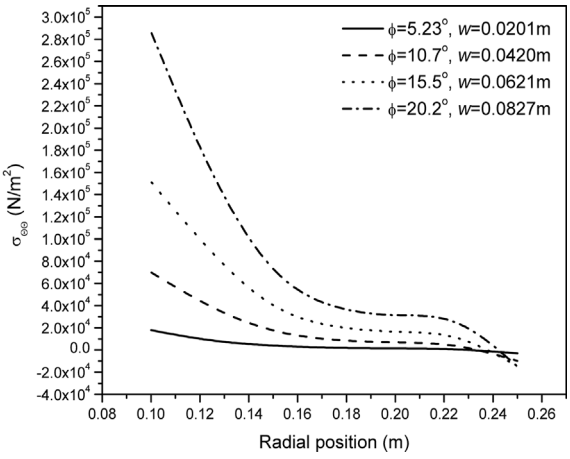

Fig. 19 Circumferential stress versus radius for different angles of twist and axial displacements

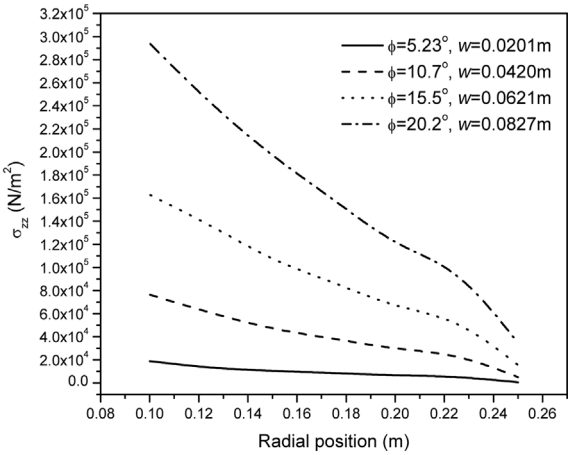

Fig. 20 Axial stress versus radius for different angles of twist and axial displacements

4. Conclusions

A three dimensional finite element model based on displacement formulation is proposed for the analysis of structural component made of rubber-elastic material. It includes geometric nonlinearity based on an updated Lagrangian approach. An efficient compressible stain energy function is used for the constitutive relationship of the rubber elastic material. A twenty node three dimensional brick element having the three usual degrees of freedom at each node is used for the finite element modeling. The model is applied to some problems having basic modes of deformation such as simple tension, pure shear, simple shear and pure bending. The results obtained are validated with the analytical results, which show a very good performance of the proposed model in terms of solution accuracy. In the present study, the Poison's ratio up to a value of 0.49932 is used where any numerical disturbance such as stability, convergence or other problem are not faced. Finally, two new problems - one having combined modes of deformation consisting of compression, bending and shear and the other one being hollow cylinder under combined torsion and telescopic shearing are solved. The new results obtained are reported for future references since the number of available results for theses problems is very few. Based on the performance of this straightforward displacement model observed in the present study, it can be highly recommended for the analysis of nearly incompressible materials undergoing deformation up to a large extent.

References

Argyris, J.H., Dunne, P.C., Angelopoulos, T. and Bichat, B. (1974), "Large natural strains and some special difficulties due to non-linearity and incompressibility in finite elements", *Comput. Methods Appl. Mech. Eng.*, **4**, 219-278.

Askes, H., Kuhl, E. and Steinmann, P. (2004), "An ALE formulation based on spatial and material settings of continuum mechanics, Part 2: Generic hyperelastic formulation", *Comput. Methods Appl. Mech. Eng.*, **193**, 4223 -4245.

Bathe, K.J. (1982), *Finite Element Procedures in Engineering Analysis*, Prentice Hall, Englewood Cliffs.

Beatty, M.F. (1987), "Topics in finite elasticity: Hyperelasticity of rubber, elastomers, and biological tissues – with examples", *Appl. Mech. Rev.*, **40**, 1699-1734.

Belytschko, T., Lu, Y.Y. and Gu, L. (1994), "Element-free Galerkin methods", *Int. J. Numer. Methods Eng.*, **37**, 229 -256.

Chen, J.-S. and Pan, C. (1996), "A pressure projection method for nearly incompressible rubber hyperelasticity, Part I: Theory", *J. Appl. Mech.*, ASME, **63**, 862-868.

Chen, J.S., Yoon, S., Wang, H.P. and Liu, W.K. (2000), "An improved reproducing kernel particle method for nearly incompressible finite elasticity", *Comput. Methods Appl. Mech. Eng.*, **181**, 117-145.

Cheng, J.-S. and Wu, C.-T. (1996), "A pressure projection method for nearly incompressible rubber hyperelasticity, Part II: Applications", *J. Appl. Mech.,* ASME, **63**, 869-876.

Cook, R.D., Malkus, D.S., Plesha, M.E. and Witt, R.J. (2001), *Concepts and Applications of Finite Element Analysis*, J. Wiley & Sons, New York, 4th Edition.

Crisfield, M.A. (1981), "A fast incremental/iterative solution procedure that handles "snap-through"", *Comput. Struct.*, **13**, 55-62.

De Souza Neto, E.A. and Feng, Y.T. (1999), "On the determination of the path direction for arc-length methods in the presence of bifurcations and 'snap-backs'", *Comput. Methods Appl. Mech. Eng.*, **179**, 81-89.

Gadala, M.S. (1992), "Alternative methods for the solution of hyperelastic problems with incompressibility", *Comput. Struct.*, **42**, 1-10.

Gent, A.N. (2001), *Engineering with Rubber*, 2nd Edition, Hanser Publishers.

Hermmann, L.R. (1965), "Elasticity equations for incompressible and nearly incompressible materials by a

variational theorem", *AIAA J.*, **3**, 1896-1900.
Hinton, E. and Campbell, J.S. (1974), "Local and global smoothing of discontinuous finite element functions using a least squares method", *Int. J. Numer. Methods Eng.*, **8**, 461-480.
Kuhl, E., Askes, H. and Steinmann, P. (2004), "An ALE formulation based on spatial and material settings of continuum mechanics, Part 1: Generic hyperelastic formulation", *Comput. Methods Appl. Mech. Eng.*, **193**, 4207 -4222.
Liu, W.K., Chang, H., Chen, J.S. and Belytschko, T. (1988), "Arbitrary Lagrangian Eulerian Petrov-Galerkin finite elements for nonlinear continua", *Comput. Methods Appl. Mech. Eng.*, **68**, 259-310.
Liu, W.K., Chen, J.S. and Zhang, Y.F. (1991), "Adaptive ALE finite elements with particular reference to external work rate on frictional interface", *Comput. Methods Appl. Mech. Eng.*, **93**, 189-216.
Masud, A. and Xia, K. (2005), "A stabilized mixed finite element method for nearly incompressible elasticity", *J. Appl. Mech.*, **72**, 711-720.
Monaghan, J.J. (1988), "An introduction to SPH", *Comput. Phys. Comm.*, **48**, 89-96.
Nayroles, B., Touzot, G. and Villon, P. (1992), "Generalizing the finite element method: Diffuse approximation and diffuse elements", *Comput. Mech.*, **10**, 307-318.
Obata, Y. (1974), PhD Thesis, School of Engineering, Kyoto University, Japan.
Ogden, R.W. (1972), "Large deformation isotropic elasticity-on the correlation of theory and experiment for incompressible rubber-like solids", *Proc. R. Soc. London*, **A 326**, 565-584.
Ogden, R.W. (1984), *Non-linear Elastic Deformations*, Ellis Horwood, Chichester.
Peng, S.H., Shimbori, T. and Naderi, A. (1994), "Measurement of elastomer's bulk modulus by means of a confined compression test", *Rubber Chem. Technology*, **67**, 871-879.
Peng, S.H. and Chang, W.V. (1997), "A compressible approach in finite element analysis of rubber-elastic materials", *Comput. Struct.*, **62**, 573-593.
Sulsky, D., Chen, Z. and Schreyer, H.L. (1994), "A particle method for history-dependent materials", *Comput. Methods Appl. Mech. Eng.*, **118**, 179-196.
Sussman, T. and Bathe, K.J. (1987), "A finite element formulation for nonlinear incompressible elastic and inelastic analysis", *Comput. Struct.*, **26**, 357-409.
Treloar, L.R.G. (1944), "Stress-strain data for vulcanized rubber under various types of deformation", *Trans. Fraday Soc.*, **40**, 59-70.
Zidi, M. and Cheref, M. (2002), "Finite deformations of a hyperelastic, compressible and fibre reinforced tube", *European Journal of Mechanics A/Solids*, **21**, 971-980.
Zienkiewicz, O.C. (1977), *The Finite Element Method*, 3rd Edn. Mc-Graw-Hill, New York.